

# Material characterisation of Cross Laminated Timber using experimental wave velocities

Simon Mecking, Ulrich Schanda

Laboratory for Sound Measurement LaSM, University of Applied Sciences Rosenheim, Germany.

Stefan Schoenwald

Laboratory for Acoustics and Noise Control, Empa - Swiss Federal Laboratories for Material Science and Technology, Dübendorf, Switzerland.

## Abstract

In multi story buildings the use of Cross Laminated Timber (CLT) is increasing. Therefore, sound insulation requirements have to be met and the prediction of sound insulation for this construction type is necessary. With the exception of low frequencies, Statistical Energy Analysis (SEA) is used in building acoustics for this purpose, which requires material properties as input data. The material characterisation of Cross Laminated Timber is a challenge. On the one hand, the composite material consists of several layers of boards; on the other hand, wood itself is inhomogeneous, anisotropic and has a low shear modulus. Differences in the manufacturing process such as the use of glue and grooves also have an impact on the overall rigidity of the plate. A characterisation based on thin plate theory is insufficient for the frequency range of building acoustics. One possibility to address this challenge is the experimental determination of frequency dependent phase velocities of bending waves in a plate that account for the above-mentioned effects. From the wave velocities the modal density used in SEA can be calculated very efficiently. This contribution focus on the time-of-flight method and phase difference method to determine phase velocities. In a case study, the direction-dependent global stiffness parameters were determined using first shear deformation theory. The measurement conditions and evaluation procedures are discussed.

PACS no. 62.65.+k, 62.30.+d

## 1. Introduction

For the calculation of structure-borne sound propagation in the building acoustic frequency range the experimental determination of phase velocities in CLT is presented; previous work can be found in [1–6]. Other methods are also available for this purpose, such as Spatial Fourier Transform of the vibration field [7–9] or updating a FE model or an experimental modal analysis [4, 10], but these will not be addressed herein.

The resulting material parameters from modal methods are based on the low frequency range behaviour and are not necessarily suitable for higher frequencies. In the low frequency range, the sensitivity of the shear modulus to the apparent bending waves is negligible (Fig.1). This can lead to strong deviations within a model update. Also differences in the boundary conditions between model acceptance and experiment.

In methods based on the elastic properties of a pure piece of wood and using the composite theory in order to draw conclusions about the properties of the CLT, it is particularly difficult to take the global shear effect into account.

Figure 1 shows that the shear influence on apparent bending waves of a CLT plate is significantly more pronounced in the building acoustic frequency range compared to a concrete plate of the same thickness. This is due to the low shear modulus typical of wood.

## 2. Theory

### 2.1. Modal density

In SEA the modal density  $n$  is the central parameter to describe the energy content of a subsystem. Generally, modal density in s/rad is found by differentiating the number of modes  $N$  with respect to the angular frequency  $\omega$

$$n(\omega) = \frac{\partial N}{\partial k} \frac{\partial k}{\partial \omega}. \quad (1)$$

In [11] an asymptotically equal calculation of modal density is described for a particular wave type of a two-dimensional system, e.g. a plate.

$$n^{2D}(\omega) \simeq \frac{S}{2\pi} \frac{\omega}{c} \frac{1}{c_g} + \Gamma'_{BC} P \quad (2)$$

The factor  $\Gamma'_{BC}$  considers the effect of the boundary condition and  $P$  is the perimeter. With increasing frequency the influence of the boundary condition is decreasing. Lyon and DeJong [11] suggested to assume  $\Gamma'_{BC} \simeq 0$  for connected subsystems. Neglecting this term in (2) the modal density depends only on the

- geometry by using the surface area  $S$  and the
- material by using the phase velocity  $c$  of the specific wave type.

$c_g$  is called the group velocity and is explained in the next section. Equation (2) shows the importance for the knowledge of the wave velocities for the proper application of the SEA.

## 2.2. Velocity of wave propagation

In the case of a *monochromatic wave* in a solid or in a fluid, the correlation between spatial and temporal propagation is described by phase velocity (3). This can be expressed by angular frequency  $\omega$  and wave number  $k$ .

$$c = \frac{\omega}{k} = \lambda f \quad (3)$$

In the case of a *group of waves* with slightly different wave numbers the propagation velocity of the envelope of this group is given by the group velocity  $c_g$  according to (4). For a small range of wave numbers it can be interpreted as a mean velocity for the involved waves. Energy propagation occurs with the group velocity.

$$c_g = \frac{\partial \omega}{\partial k} = c + \frac{\partial c}{\partial k} k \quad (4)$$

Usually the wave velocity is dependent on the wave number; this dependency is called dispersion. Only in the non-dispersive case the group velocity equals the phase velocity. The wave types of an isotropic plate are explained below.

### 2.2.1. Quasi-longitudinal waves

These waves can be assumed as non-dispersive below a certain wave number, where the wavelength is much greater than the plate thickness. At this *acoustic thin plate* condition the phase velocity is given by (5).

$$c_L = \sqrt{\frac{E}{\rho(1-\mu^2)}} \quad (f < f_L) \quad (5)$$

The corresponding high frequency limit  $f_L$  for this assumption is described in e.g. [12, 13].

### 2.2.2. Transverse shear waves

These waves are non-dispersive as well. The phase velocity in (6) depends on shear modulus  $G$  and density  $\rho$ .

$$c_T = \sqrt{\frac{G}{\rho}} \quad (6)$$

### 2.2.3. Bending waves

These waves are dispersive. For calculation of the phase velocity of apparent bending waves the frequency range can be subdivided into three parts. Starting from an approach for acoustic thin plates, more general approaches are presented step-by-step.

**Part I** In the case of wavelength being much greater than the plate thickness  $l_3$  the phase velocity of bending waves can be calculated according classic thin plate theory (Kirchhoff).

$$c_B = \sqrt[4]{\frac{\omega^2 B_P}{\rho l_3}} = \sqrt[4]{\frac{\omega^2 l_3^2}{12}} c_L^2 \quad (f < f_B) \quad (7)$$

The frequency limit  $f_B$  is described in [13].

**Part II** For moderately thick plates the bending wave equation can be modified considering shear deformation and rotatory inertia [15]. The two approaches below take into account these influences on the phase velocities of bending waves, but differences between the low and high frequency asymptotes of the apparent bending waves are small in Figure 1.

(a) In [1, 16] an effective phase velocity of bending waves (8) is defined as combination of bending and transverse shear waves to consider the shear influence at higher frequencies. The shear stiffness and the bending stiffness is assumed to be connected in parallel. In [cf. 1] an approximation (9) is suggested with an accuracy in the range of  $\pm 1\%$  of (8).

$$c_{B\text{eff}} = \frac{c_B^2}{\kappa c_T} \sqrt{-\frac{1}{2} + \frac{1}{2} \sqrt{1 + 4 \left( \frac{\kappa c_T}{c_B} \right)^4}} \quad (8)$$

$$\approx \left( \frac{1}{c_B^3} + \frac{1}{(\kappa c_T)^3} \right)^{-\frac{1}{3}} \quad (9)$$

(b) In [12, 17, 18] the effective phase velocity of bending waves is defined as combination of bending, transverse shear and quasi-longitudinal waves according to (10).

$$c_{B\text{eff}} = \left( \frac{1}{2} \left( \frac{1}{c_L^2} + \frac{1}{\kappa^2 c_T^2} \right) \right. \quad (10)$$

$$\left. + \sqrt{\frac{1}{c_B^4} + \frac{1}{4} \left( \frac{1}{\kappa^2 c_T^2} - \frac{1}{c_L^2} \right)^2} \right)^{-0.5}$$

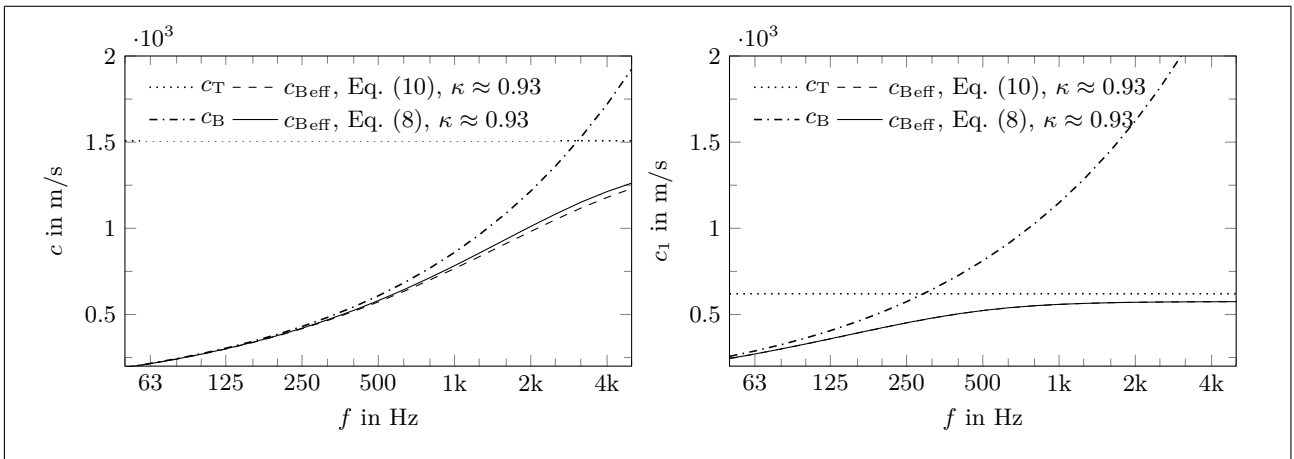


Figure 1. Shear influence on the phase velocities of apparent bending waves  $c_{B,eff}$  of a concrete plate (left) with  $E = 13.6$  GPa,  $\mu = 0.3$  and  $\rho = 2300$  kg/m<sup>3</sup> [14] in comparison to a Cross Laminated Timber plate (right) in the principal direction with  $E_1 = 8.24$  GPa,  $\mu_{13,31} = 0.3$  and  $\rho = 450$  kg/m<sup>3</sup>. The thickness is approximately 0.16 m in both cases.

**Part III** For very small wavelengths compared to the plate thickness, the wave velocity changes asymptotically to the surface wave velocity. Lord Rayleigh [19] calculated for the first time for an elastic half space this surface wave velocity, the so-called Rayleigh wave velocity  $c_R$ . It is slightly slower than the transverse shear wave velocity (11) [cf. 15, 19].

$$c_R = \kappa c_T \quad (11)$$

Depending on the Poisson ratio  $\mu$  the refractive index  $\kappa$  can be calculated by (12) [cf. 15, 19].

$$(2 - \kappa^2)^2 = 4 \sqrt{(1 - \alpha \kappa^2)(1 - \kappa^2)} \quad \text{with} \quad (12)$$

$$\alpha = \frac{c_T^2}{c_{L,pure}^2} = \frac{1 - 2\mu}{2(1 - \mu)} \quad (13)$$

In (13) the constant phase velocity of pure longitudinal waves  $c_{L,pure}$  is used. For the range of Poisson's ratio  $[0 < \mu \leq 0.5]$  the results are in the range  $[0.874 \lesssim \kappa \lesssim 0.955]$ .

The difference between transverse shear wave velocity and the surface wave velocity was neglected in [1] for (8) and (9) and in [17] for (10), which corresponds to use  $\kappa = 1$ . The difference was considered in [12, 13, 15, 20, 21] by using the Rayleigh surface wave velocity as high frequency asymptote.

### 3. Experiment

#### 3.1. Set-up

In a case study a 3-ply CLT panel, mounted in a heavy test frame was measured. The identical plate was already subject of an earlier study two years ago [23], which is called *experiment 1*. The new measurement is defined as *experiment 2*. The set-up of experiment 1 is the same as described in [2], but for another CLT

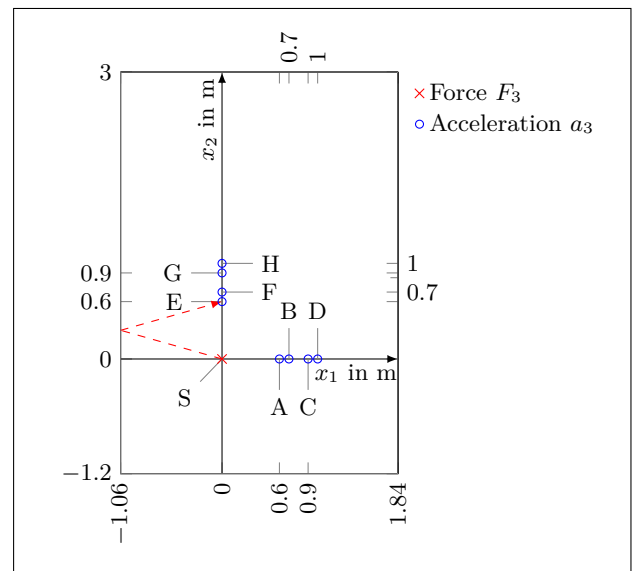


Figure 2. Excitation and observer positions of the measurement to determine the phase velocities. The 3-ply CLT plate with the dimensions  $2.90 \text{ m} \times 4.20 \text{ m} \times 0.10 \text{ m}$  and  $\rho = 484$  kg/m<sup>3</sup> is identical to the one in [22]. The layer thicknesses are 30 mm, 40 mm and 30 mm.

panel. The dimensions of the panel, the source position of the shaker and the positions of the accelerometers are shown in Figure 2. The measurement was always executed perpendicular to the plate plane in direction  $x_3$ . In the following, therefore, only  $a$  is used instead of  $a_3$ . The positions must be sufficiently apart from the source to prevent measurement in the near field range and from the edges of the panel so that the first reflection (red path in Fig. 2 for Position E) is not present too early in the time signal of the accelerometers at low frequencies. These positions are the same in both experiments, but there are some differences between the used measurement equipment and set-up listed in Table I.

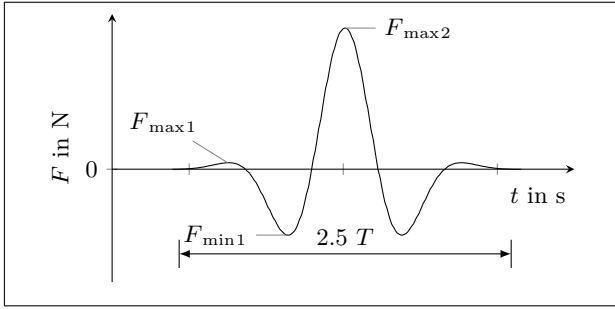


Figure 3. Sinusoidal pulse with Hanning windowing as predefined excitation signal.

In order to ensure that high frequencies can also be excited, the shaker attachment should be designed in such a way that eigen frequencies, e. g. by the stinger, are above the frequency range of interest. The diameter of the contact surface between attachment of the shaker and the panel should be smaller than one sixth of the expected bending wavelength [cf. 12] to enable the excitation of high frequencies.

As mentioned in section 2.2.3, bending waves are dispersive, therefore the measurement is performed for individual frequencies. For both experiments short sinusoidal pulses (Fig.3) were used with 2.5 cycles and were smoothed with a Hanning window. In fact, it does not excite a single frequency, but rather a narrow frequency band. But if the frequency band is very narrow, the influence of the dispersion in this band can be neglected. For this reason it is necessary to use a smooth fade in of the sinusoidal excitation signal. Furthermore an additional broad excitation due to an excessively abrupt transition is avoided. The time resolution of the excitation signal should be high enough to represent a sinusoidal period through many data points even at the highest frequency of interest.

For an efficient measurement in experiment 2, an excitation signal was generated by incorporating the individual pulses for the different frequencies one after the other, each with a sufficient delay of about 1 s between the individual signals, so that the vibration at the accelerometers on the plate had faded out.

### 3.2. Measurement evaluation

#### 3.2.1. Pre-processing of raw data

Before the main evaluation with the time-of-flight (ToF) or the phase difference (PhD) method, the raw time data is preprocessed in the same way. The sign definition must be equal for both time signals. First the background noise is found as the the median within the time window  $[t_{BN,start}, t_{BN,end}]$  and the entire time signal is corrected by this value to ensure there is no offset.

For processing only a short duration at the beginning of the active vibration signal is used, as reflections by the plate edges occur very early due to the finite dimensions of the plate. In order to determine

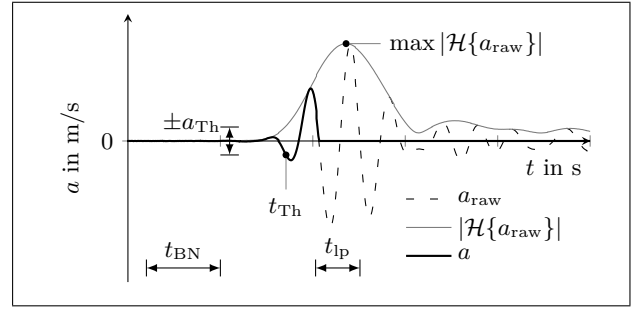


Figure 4. Time window selection for a measured acceleration  $a_{raw}$  using a low pass filter in the time domain.

the approximate arrival time  $t_{Th}$  of the active vibration, the exceeding of a threshold value  $a_{Th}$  for the acceleration is used (Fig. 4). In order to determine the threshold value, the envelope of the time signal is first formed using the magnitude of the Hilbert transformation of  $a_{raw}$ . The product of force amplitude ratio  $\beta$  of the predefined excitation signal in Figure 3 and the first significant maximum of the envelope of the acceleration gives the threshold value (14).

$$a_{Th} = \beta \max |\mathcal{H}\{a_{raw}\}| \quad (14)$$

with  $\left( \frac{F_{max1}}{F_{max2}} < \beta < \frac{|F_{min1}|}{F_{max2}} \right)$

$$\mathcal{H}\{a_{raw}\} = a_{raw} * \frac{1}{\pi t} \quad (15)$$

From this approximate start time, a time window for processing is defined. The duration is dependent on the excitation frequency. The first zero crossings are searched within this time window  $t_{ip}$  (Fig. 4). The zero crossings that take place for both sensors with the same sign change are set as the end point of the analysis. Any signal that occurs afterwards is replaced by zeros. It can be interpreted as a low pass filter in time domain to avoid the influence of reflections as far as possible.

#### 3.2.2. Time-of-flight method

Using this method the phase velocity in direction  $i$  is calculated directly from the spacing  $d$  between two measuring positions X and Y to the time delay  $\tau$  of the phase between the time signals according to (16), if X, Y and the source position S are on the same path (cf. Fig.2).

$$c = \frac{d(X, Y)}{\tau(a_X, a_Y)} \quad (t < t_{Reflection}) \quad (16)$$

To calculate the time delay of the discrete time signals, characteristic features such as peak-to-peak or zero crossings can be used. However, small noise levels in the signal can have a significant influence on the result. A much more robust method is cross correlation, since it is based on more information than individual data points.

Table I. Measurement equipment and set-up used to determine the phase velocities.

	Experiment 1 [2, 23]	Experiment 2
Data acquisition Sample rate	NATIONAL INSTRUMENTS® 120 000 Hz	Müller-BBM VibroAkustik Systeme GmbH, PAK MKII 102 400 Hz
Accelerometer Sensitivity	PCB PIEZOTRONICS <sup>INC.</sup> , 353B15 (10 ± 1) mV/g	Brüel & Kjær, 4513-B-002 (500 ± 50) mV/g
Shaker Excitation signal Preset excitation	[100:20:3000] Hz	Brüel & Kjær, 4809 sinusoidal pulses (2.5 cycles), Hanning windowed [100:160:3000] Hz

It is used here with the MATLAB® function *xcorr.m* to calculate the time delay  $\tau$  from the maximum of the cross correlation between both prepared time signals in (17) and (18) according section 3.2.1.

$$R_{XY}(L) = \left( a_X \star a_Y \right)(L) \quad (17)$$

$$\tau(a_X, a_Y) = \frac{L(\max R_{XY})}{f_s} \quad (18)$$

Thereby  $L$  represents the number of shifted samples of the discrete cross correlation.

### 3.2.3. Phase difference method

An alternative method to determine phase velocities is the PhD method. According to [1, 2] the results of this method are more reliable at low frequencies as results from the ToF method.

$$c = \omega \frac{d(X, Y)}{|\phi(\underline{a}_X, \underline{a}_Y)|} \quad (t < t_{\text{Reflection}}) \quad (19)$$

Before calculating the phase difference  $\phi$  in the denominator of (19), the MATLAB® function *unwrap.m* is applied to the phase angles of both complex signals. It corrects the radian phase angles by adding multiples of  $\pm 2\pi$  at phase changes between consecutive elements of the signals greater than or equal to a phase change tolerance of  $\pi$  radians. For the distance  $d$  of the sensors no spatial but a temporal sampling theorem must be considered, because the temporal wave and not the spatial wave is used in this method.

## 3.3. Limitations and uncertainties

### 3.3.1. Limitations

For low frequencies, the requirement on the minimal time window is in conflict with the requirement to avoid edge reflections in the signal to be analysed. Depending on the difference of the arrival time of the wave front at the sensor from the shortest indirect path to the direct path (Fig. 2), the time signal without reflection is too short to be evaluated according to the procedure in section 3.2.

For high frequencies, additional oscillations can superpose the signals to be analysed. These can be caused by

- thickness resonances,
- resonances of sensor attachment or
- reflections on impedance discontinuities.

For the ToF as well as for the PhD method a possible phase offset between the channels used in the measurement should be taken into account. Furthermore, the relative uncertainty of the phase velocity results from different input quantities according (20) or (21) and are explained in the following subsections.

$$u_{c,\text{ToF}} = \sqrt{u_d^2 + u_\tau^2} \quad (20)$$

$$u_{c,\text{PhD}} = \sqrt{u_d^2 + u_\phi^2 + u_f^2} \quad (21)$$

### 3.3.2. Frequency

The relative uncertainty  $u_f$  in the determination of the frequency of the sinusoidal signal by means of Fourier transformation in (23) is due to the finite time signal with duration  $T_{\text{tot}}$  and is given by (22).

$$u_f = \frac{1}{T_{\text{tot}} f} \quad (22)$$

It is necessary that a sufficient length of a vibration above noise is contained in the time signal. This kind of uncertainty decreases with increasing frequency and is negligible if  $T_{\text{tot}}$  is set sufficiently high by zero padding.

If the frequency is not determined directly from the time signal but rather from the pre-defined excitation signal, considerable deviations can occur as a systematic deviation. These can partly be attributed to the dynamic properties of the structure or the shaker attachment. At low frequencies where the degree of dispersion is higher and the modal density is lower, this deviation can be significant (cf.  $c_L$  in Tab. II).

Another aspect is the dispersion due to the effectively excited frequency bandwidth, which is not infinitely narrow. Thus, slightly different frequencies are determined for the two time signals according to (23) in the Fast Fourier Transform (FFT) spectrum. To minimise this blur on the dispersion relationship the

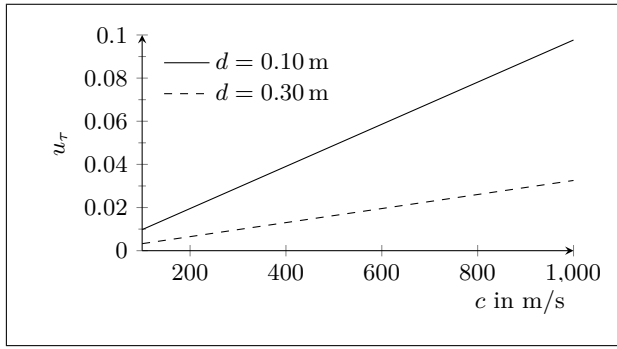


Figure 5. Relative uncertainty only due to time discretisation  $u_\tau$  depending on the phase velocity  $c$  and distance  $d$  at a sampling rate  $f_s = 102\,400$  Hz.

arithmetic mean of these is used as approximately effective excitation frequency  $\bar{f}$  in (24).

$$f = \max |\mathcal{F}\{a\}| \quad (23)$$

$$\bar{f} = \frac{f_X + f_Y}{2} \quad (24)$$

### 3.3.3. Distance

The relative uncertainty in distance is given by (25).

$$u_d = \frac{2\Delta d}{d} \quad (25)$$

$\Delta d$  is the accurateness of determining the distance of the position of the accelerometers. A deviation in the distance leads to a systematic deviation in the entire dispersion relationship.

### 3.3.4. Time delay

The relative uncertainty of the time delay  $u_\tau$  is determined by the sampling rate  $f_s$  of the measuring system and the time delay  $\tau$  between the two measuring positions according to (26).

$$u_\tau = \frac{1}{f_s \tau} = \frac{1}{f_s} \frac{c}{d} \quad (26)$$

For the actual sampling rate of experiment 2 the correlation between relative uncertainty, phase velocity and distance is shown in Figure 5.

### 3.3.5. Phase difference

If the distance of the accelerometer is fixed the relative uncertainty  $u_\phi$  depends on several factors like the wavelength, the sampling rate and the time window length. Since it also depends on the representation of the vibration, it is not straightforward to quantify.

## 3.4. Regression analysis

Based on the relationships of the phase velocities of apparent bending waves in section 2.2.3 two equations are used to fit the phase velocities of surface waves  $c_R$  and the quasi-longitudinal waves  $c_L$ .

(a) By inserting (6) and (7) in (8) equation (27) can be derived.

$$c_{\text{Beff}} = \frac{c_L}{c_R} \sqrt{\frac{\omega^2 l_3^2}{12}} \sqrt{-\frac{1}{2} + \sqrt{\frac{1}{4} + \frac{c_R^4}{c_L^2} \frac{12}{\omega^2 l_3^2}}} \quad (27)$$

(b) Inserting them in (10), equation (28) is obtained.

$$c_{\text{Beff}} = \left( \frac{1}{2} \left( \frac{1}{c_R^2} + \frac{1}{c_L^2} \right) + \sqrt{\frac{12}{\omega^2 l_3^2 c_L^2} + \frac{1}{4} \left( \frac{1}{c_R^2} - \frac{1}{c_L^2} \right)^2} \right)^{-0.5} \quad (28)$$

To minimise the influence of single outliers, bisquare weights are used as a robust regression method. Due to the limitations in section 3.3.1, the frequency range for the fit is limited to both low and high frequencies. The confidence level of the fit results is  $\alpha = 95\%$ .

## 4. Results

The constant settings for the evaluation process are  $t_{\text{BN}} = [0.6T, 1.5T]$ ,  $\beta = 1/7$  and  $d = (300 \pm 2)$  mm. For this value of  $d$  the relative distance uncertainty is negligible ( $u_d \leq 0.7\%$ ) and the relative uncertainty of time delay is  $u_\tau \leq 3\%$  according to Figure 5. The relative uncertainty for the frequency determination using the FFT is  $u_f \leq 1\%$  for  $f \geq 400$  Hz in case of  $T_{\text{tot}} = 0.25$  s according (23). The frequency range for all regression analyses is limited to  $f[400, 2500]$ . The uncertainties of the individual data points are neglected for the regression.

In Figure 6 the results of the two experiments are compared. Despite the two years between the two experiments, different experimenters and partly different measurement techniques (Tab.I), the reproducibility is significantly high. It also indicates the robustness of the evaluation process. The significant deviation above 1 kHz is due to an overload in the raw data of experiment 1.

One hypothesis for the outliers in Figure 6 on the right at  $f \geq 2.7$  kHz is that the intersections between the individual boards forming the top layer of CLT represent impedance discontinuities in direction  $x_2$  as soon as the board spacing is greater than half the wavelength. In this case the propagation of surface waves would be influenced by reflections and the evaluation according to section 3.2 would fail.

Figure 7 shows the equivalent results to Figure 6 on the left but using the ToF method. The quasi-longitudinal phase velocity determined by the ToF method is significantly higher. This does not hold for the velocity of the surface waves. When estimating the modulus of elasticity, the use of the fitted  $c_{L,i}$  from the PhD method leads to more plausible results. The error bars in Figure 7 show resulting uncertainties according

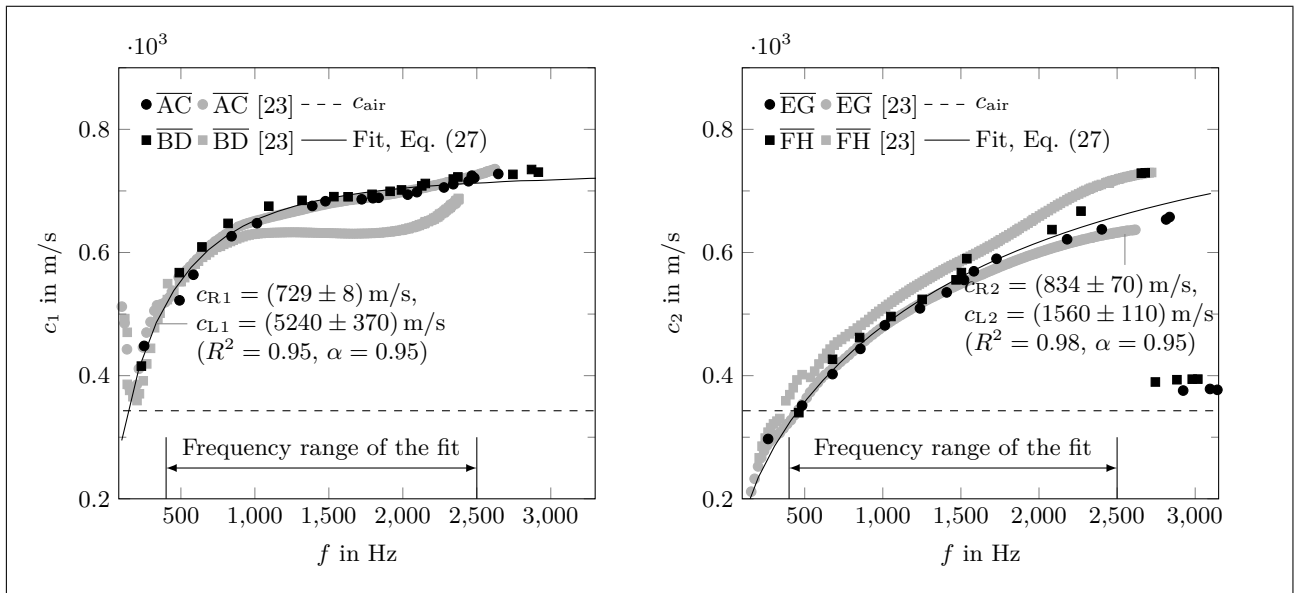


Figure 6. Phase velocities of apparent bending waves using the *phase difference (PhD)* method, applied to the time raw data of experiment 1 (grey) and 2 (black) of the identical Cross Laminated Timber plate with  $l_3 = 100$  mm.

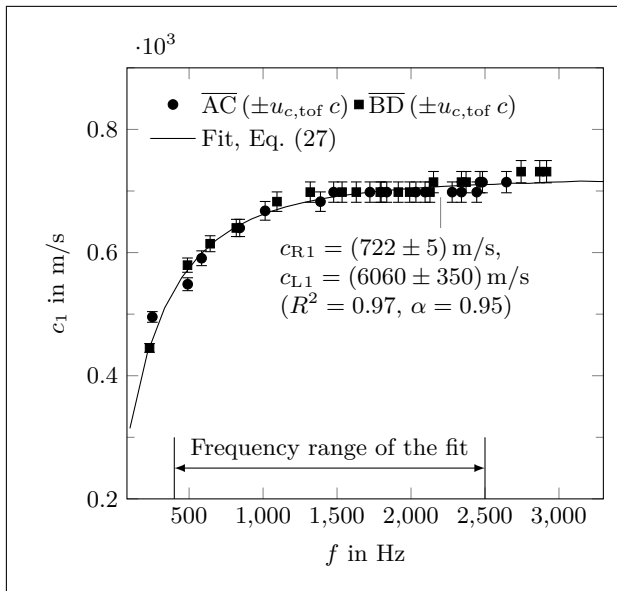


Figure 7. Phase velocities of apparent bending waves using *time-of-flight (ToF)* method of experiment 2. The bars represents the uncertainties according (20).

(20) caused by time discretisation and distance. The absolute uncertainties are increasing with frequency.

Table II gives an overview of variants of the regression analysis regarding the input data from the evaluation methods and frequency allocation. Only results according to (27) are shown, since these results differ only slightly from those according to (28). All variants using the PhD method show lower quasi-longitudinal wave velocities. The procedure of frequency allocation has an influence on the quality of the regression. In case of a strong dispersion ( $x_2$ ), the frequency result-

ing from a FFT leads to a higher degree of determination.

## 5. Conclusions

The determination of the phase velocity of apparent bending waves is possible by using the phase difference method and the time of flight method.

Overall, the results of the two methods show a high degree of agreement with the exception at low frequencies where the phase difference method leads to more plausible results. The frequency of the signal at the accelerometer should be determined from a FFT rather than using the defined of the input signal for excitation.

With regression models the direction-dependent and frequency-independent phase velocities of quasi-longitudinal waves and surface waves can be determined with high fit qualities. For the current data set a large part of the building acoustic frequency range could be covered. The shear effect has a decisive influence on the apparent bending waves of wood materials such as CLT in this frequency range. The velocity of the surface waves takes this shear effect into account. These issues demonstrate the advantages of material characterisation using the wave velocities  $c_{L,i}$  and  $c_{R,i}$  for application in the SEA. To calculate the modal density in (2) the geometric mean of the direction dependent phase velocities and group velocities can be used [cf. 11]. The calculation of the elastic constants ( $E_i, G_{ij}$ ) leads to an increase in uncertainties, since additional direction dependent input variables such as Poisson's ratios and refractive indices of surface to transverse shear waves  $\kappa_i$  are necessary but often not known for a composite material such as CLT.

Table II. Results of the regression analysis with confidence level  $\alpha$  for phase velocities of quasi-longitudinal and surface waves in case of experiment 2 for direction  $i$ . The abbreviations are phase difference (PhD) method, time-of-flight (ToF) and pre-defined excitation frequency (pd). The relative uncertainty due to the confidence interval is also given.

$i$	Method	$f$	$c_{Ri}$ in m/s with $\alpha = 0.95$	$u_{cR,\alpha}$	$c_{Li}$ in m/s with $\alpha = 0.95$	$u_{cL,\alpha}$	$R^2$
1	PhD	FFT		0.01		0.07	0.95
1	ToF	FFT		0.01		0.06	0.97
1	PhD	pd		0.01		0.07	0.96
1	ToF	pd		0.01		0.08	0.94
2	PhD	FFT		0.08		0.07	0.98
2	ToF	FFT		0.08		0.08	0.98
2	PhD	pd		0.15		0.15	0.92
2	ToF	pd		0.10		0.15	0.91

**Acknowledgement**

The authors would like to thank A. Santoni for sharing raw data of his measurements and B. van Damme and H. M. Tröbs for support during the measurements performed at Laboratory for Acoustics and Noise Control, Empa - Swiss Federal Laboratories for Material Science and Technology, Dübendorf, Switzerland.

**References**

[1] J. H. Rindel: Dispersion and absorption of structure-borne sound in acoustically thick plates. *Appl Acoust* 41.2 (1994), pp. 97–111.

[2] A. Santoni et al.: Determination of the elastic and stiffness characteristics of cross-laminated timber plates from flexural wave velocity measurements. *J Sound Vib* 400 (2017), pp. 387–401.

[3] T. R. T. Nightingale et al.: Estimating In-Situ Material Properties of a Wood Joist Floor: Part 1 – Measurements of the Real Part of Bending Wavenumber. *Build Acoust* 11.3 (2004), pp. 175–196.

[4] A. Gülzow: Zerstückungsfreie Bestimmung der Biegesteifigkeit von Brettsperholzplatten. Dissertation. ETH Zürich, 2008.

[5] N. H. Clark and S. Thwaites: Local phase velocity measurements in plates. *J Sound Vib* 187.2 (1995), pp. 241–252.

[6] I. Roelens et al.: In situ measurement of the stiffness properties of building components. *Appl Acoust* 52.3-4 (1997), pp. 289–309.

[7] C. Winter: Messtechnische Untersuchung leichter Deckentragwerke im Wellenzahlbereich und Prognose der abgestrahlten Schalleistung. TU Munich, 2012.

[8] M. Kohrmann: Numerical Methods for the Vibro-Acoustic Assessment of Timber Floor Constructions. PhD thesis. TU Munich, 2017.

[9] B. Van Damme and A. Zemp: Measuring Dispersion Curves for Bending Waves in Beams: A Comparison of Spatial Fourier Transform and Inhomogeneous Wave Correlation. *Acta Acust United Ac* 104.2 (2018), pp. 228–234.

[10] A. Paolini et al.: A high-order finite element model for vibration analysis of cross-laminated timber assemblies. *Build Acoust* 24.3 (2017), pp. 135–158.

[11] R. H. Lyon and R. G. DeJong: Theory and application of statistical energy analysis. 2nd ed. Newton, MA, USA: Butterworth-Heinemann, 1995.

[12] L. Cremer and M. Heckl: Körperschall. Berlin: Springer, 1996.

[13] C. Hopkins: Sound Insulation. Butterworth-Heinemann, 2007.

[14] S. Ljunggren: Airborne sound insulation of thick walls. *J Acoust Soc Am* 89.5 (1991), pp. 2338–2345.

[15] R. D. Mindlin: Influence of rotatory inertia and shear on flexural motions of isotropic, elastic plates. *J Appl Mech* 18 (1951), pp. 31–38.

[16] G. Kurtze and B. G. Watters: New wall design for high transmission loss or high damping. *J Acoust Soc Am* 31.6 (1959), pp. 739–748.

[17] D. B. Pedersen: Estimation of Vibration Attenuation through Junctions of Building Structures. *Appl Acoust* 46 (1995), pp. 285–305.

[18] N. V. Movchan et al.: Flexural waves in structured elastic plates: Mindlin versus bi-harmonic models. *Proc Royal Soc Lond* 467.2127 (2011), pp. 869–880.

[19] J. W. S. Rayleigh: On Waves Propagated along the Plane Surface of an Elastic Solid. *Proc Lond Math Soc* s1-17.1 (1885), pp. 4–11.

[20] A. Meier: Die Bedeutung des Verlustfaktors bei der Bestimmung der Schalldämmung im Prüfstand. PhD thesis. RWTH Aachen, 2000.

[21] R. J. M. Craik: Sound transmission through buildings: Using Statistical Energy Analysis. Aldershot, England and Brookfield, Vt., USA: Gower, 1996.

[22] A. Santoni: Sound radiation and sound transmission in building structures. PhD thesis. University of Ferrara, 2016.

[23] A. Santoni: Measurement of the phase velocities on a 3-ply Cross Laminated Timber plate with a thickness of 100 mm. Unpublished raw data measured at Empa in Dübendorf, Switzerland. 2015.